Current Applied Physics 19 (2019) 394–399

Contents lists available at ScienceDirect

Current Applied Physics

journal homepage: www.elsevier.com/locate/cap

Cu_2S nanocrystals incorporated highly efficient non-fullerene ternary organic solar cells

Govinda Lakhotiya[a,b,*], Namdeo Belsare[b], Abhimanyu Rana[c], Vinay Gupta[d,**]

[a] Department of Physics, Jankidevi Bajaj College of Science (Autonomous), Wardha 442001, India
[b] Department of Physics, Vidyabharati Mahavidyalaya, Amravati 444602, India
[c] School of Engineering and Technology, BML Munjal University, Haryana 122413, India
[d] Advanced Materials and Devices Division, CSIR-National Physical Laboratory, New Delhi 110012, India

ARTICLE INFO

Keywords:
Cu_2S nanocrystals
Organic solar cells
PBDB-T
ITIC
Photo electrochemical impedance spectroscopy

ABSTRACT

Here, we report Cu_2S nanocrystals based non-fullerene ternary polymer solar cells by incorporating Cu_2S in conjugated polymer (PBDB-T: poly[(2,6-(4,8-bis(5-(2-ethylhexyl)thiophen-2-yl)-benzo[1,2-b:4,5-b′]dithiophene))-alt-(5,5-(1′,3′-di-2-thienyl-5′,7′-bis(2-ethylhexyl) benzo[1′,2′-c:4′,5′-c′]dithiophene-4,8-dione))]) and small molecule non-fullerene compound (ITIC:3,9-bis(2-methylene-(3-(1,1-dicyanomethylene)-indanone))-5,5,11,11-tetrakis(4-hexylphenyl)-dithieno[2,3-d:2′,3′-d′]-*s*-indaceno[1,2-b:5,6-b′]dithiophene). The devices were fabricated in inverted configuration i.e. ITO/ZnO/PBDB-T: Cu_2S NCs: ITIC/MoO_3/Ag. Effect of concentration of Cu_2S nanocrystals on the performance parameters of PBDB-T: ITIC based organic solar cells is studied. An enhancement in the power conversion efficiency from 8.24% to 9.53% is achieved for the optimum concentration of Cu_2S nanocrystals in the organic photoactive blend. The cause of improvement in the performance parameters of the device is investigated by means of the light intensity dependent electrochemical impedance spectroscopy and atomic force microscopy. It is found that the devices with Cu_2S nanocrystals have less trap-assisted recombination.

1. Introduction

It is well known that in comparison to conventional silicon-based solar cells, third generation solar cells which includes dye-sensitized solar cells (DSSCs), bulk-heterojunction organic/polymer solar cells (OSCs/PSCs), organic-inorganic hybrid solar cells (HSCs) and perovskite solar cells (PSCs) offers two main advantages: solution processability and low processing temperature [1–4]. Besides this, OSCs offer good cost-efficiency balance, short energy payback time, low-cost materials, scalable fabrication using screen printing, inkjet printing, and roll-to-roll printing, and adaptability to flexible plastic substrates and therefore are of considerable interest in the recent times [5–7]. However, their power conversion efficiency (PCE) is still behind the other members of the third generation solar cells due to the narrow band gap of donor polymer and poor mobility of carriers in both donor polymers and fullerene-based acceptors [8–10]. To overcome this, in the last two decades, new low bandgap donor polymer and high electron mobility acceptors have been developed [11–14]. Although this has helped to improve the laboratory scale OSCs with PCE > 17%, especially in case of tandem solar cells but commercialization of OSCs requires much higher PCE and stable device performance [15–20]. Fabricating a tandem OSCs is very challenging due to technical complexities as it involves multi-layer stacking, processing of a robust intermediated layer, and coupling of appropriate absorbers as well as the optimization of the active layer's thickness [21,22]. On the other hand, fabrication of ternary OSCs is a relatively better option and needs identification of the suitable third component of the ternary blend [23–26]. In some of the systems, PCE has increased and reached maxima with the optimization of the concentration of the third component in the matrix of the donor polymer and acceptor.

In general, ternary OSCs consists of photoactive layer spin-casted using ternary photoactive blend comprised of donor polymer/solution processable small molecule, fullerene/non-fullerene acceptor and the third component [25–28]. The choice of the third component is primarily done on the basis of the role expected such as cascade or parallel charge transfer, energy transfer, complementary absorption of donor polymers, in-situ light scattering, etc. [25–28]. Thus, in principle, it could be anything such as additional donor polymer, acceptor, the

* Corresponding author. Department of Physics, Jankidevi Bajaj College of Science (Autonomous), Wardha 442001, India.
** Corresponding author.
E-mail addresses: lakhotiya.govinda@gmail.com (G. Lakhotiya), drvinaygupta@netscape.net (V. Gupta).

https://doi.org/10.1016/j.cap.2019.01.006
Received 5 November 2018; Received in revised form 25 December 2018; Accepted 4 January 2019
Available online 04 January 2019

sensitizer (dye/metal, semiconductors and dielectric nanocrystals (NCs)), etc. Till date, a variety of ternary OSCs were fabricated using the third component discussed above and has shown improvement in the performance parameters. Among them, ternary OSCs with semiconducting NCs as the third component are of significant interest. Addition of semiconducting NCs brought a lot of advantages associated with semiconducting NCs such as tunable bandgap, scalable synthesis, energy band alignments that aids in exciton dissociation. Most important characteristics of NCs are its excellent charge transport, solubility in host matrix solvent and high thermal and photo-chemical stability. To exploit these advantages, semiconducting NCs of various semiconductors like CdSe, CdS, CdTe, Si, PbS, ZnO, Cu_2S, and FeS_2 have been incorporated in the photoactive blends comprised of multiple donors: acceptors systems [29–35]. However, to the best of our knowledge, there are hardly any reports on non-fullerene ternary OSCs with semiconducting NCs as the third component.

Here in, we report nanocrystals (NCs) based non-fullerene ternary polymer solar cells. For this, synthesis of Cu_2S NCs has been carried out and its effect on one of the most efficient solution processable organic solar cells (OSCs) consisting conjugated polymer (PBDB-T:poly[(2,6-(4,8-bis(5-(2-ethylhexyl)thiophen-2-yl)-benzo[1,2-b:4,5-′]dithiophene))-alt-(5,5-(1′,3′-di-2-thienyl-5′,7′-bis(2-ethylhexyl)benzo[1′,2′-c:4′,5′-c′]dithiophene-4,8-dione))]) and small molecular non-fullerene compound (ITIC: 3,9-bis(2-methylene-(3-(1,1-dicyanomethylene)-indanone))-5,5,11,11-tetrakis(4-hexylphenyl)-dithieno[2,3-d:2′,3′-d′]-*s*-indaceno[1,2-b:5,6-b′]dithiophene) has been studied. Cu_2S could be an interesting system due to low bandgap of ~1.21 eV (indirect), giving absorption over a wide spectrum in UV–Vis.–NIR region, and therefore can harness the major part of the solar spectrum [29,30]. Also, the conduction band of Cu_2S around 3.60 eV is well positioned between LUMO of donor polymer PBDB-T and fullerene free acceptor ITIC, acting as an electron cascade between them [29,30]. Thus, we synthesized Cu_2S NCs and characterized it for the phase purity and crystal structure, morphology, and optical properties. This is followed by a systematic study to investigate variation in the performance parameters of PBDB-T: ITIC OSCs with a change in the concentration of Cu_2S NCs. The obtained results were explained by means of the light intensity dependent electrochemical impedance spectroscopy and atomic force microscopy.

2. Experimental

2.1. Synthesis of Cu_2S NCs

In the present study, synthesis of Cu_2S NCs has been carried out by slightly modifying the protocol developed by Alivisatos et al. [36]. Briefly, synthesis of colloidal Cu_2S NCs involves hot injection reaction between copper(II) acetylacetonate and ammonium diethyldithiocarbamate in a mixed solvent of dodecanethiol and oleic acid. The detailed experimental procedure can be found elsewhere.

2.2. Device fabrication

Devices were fabricated following the device architecture mentioned in Fig. 3(a) and corresponding energy levels of the materials used in the fabrication are shown in Fig. 3(b). At first, a photoactive blend comprised of PBDB-T (10 mg) and ITIC (10 mg) was prepared in 1 ml of CB with 0.5% v/v of 1, 8 diiodooctane (DIO) solvent as an additive. The solution was allowed to stir at 50 °C in the dark for at least 12 h [12]. For the ternary photo-active blend, some part of ITIC is replaced by the equal amount of Cu_2S NCs. For the device fabrication, sol-gel ZnO, synthesized by the method reported elsewhere, was spin-coated on the pre-cleaned ITO coated glass substrates (with a sheet resistance of 15 Ωsq^{-1} and transmittance > 85%) at 2000 rpm for 30 s to obtain a film of ≈40 nm [37]. The substrates were annealed at 200 °C for 15 min to remove excess solvents. After that, the photoactive blend was spin-coated at 2500 rpm for 60 s to obtain a film thickness of ≈100 nm and annealed at 160 °C for 10 min. Subsequently, the devices were evaporated using the shadow mask by thermal evaporation of 10 nm MoO_3 layer as a hole transport layer and 100 nm Ag electrode as an anode.

2.3. Device characterization and testing

Keithley 2600 source meter and a Newport solar simulator (model number 91160) with AM 1.5G spectral distribution at 1000 W/m^2 intensity was used for J-V characteristics of the cells. Bentham's PVE300 was used external quantum efficiency (EQE) spectra. Using a shadow mask, the active device area of the cells was fixed as 7 mm^2. Atomic force microscopy (AFM) of the films of photoactive blends with the different wt % of Cu_2S NCs has been carried out on Nanosurf's C 3000 model.

3. Results and discussion

Before employing the synthesized Cu_2S nanocrystals (NCs) into the photoactive blend, a systematic study has been carried out to confirm phase purity and crystal structure, morphology and optical properties of the synthesized Cu_2S NCs. Fig. 1(a) depicts the X-ray diffraction pattern (Cu K_α radiation, λ = 1.5418 A°, Rigaku's MiniFlex 600) of as-synthesized Cu_2S NCs employed at a scanning rate of 5°/min in the 2θ range from 20° to 80°. Presence of all the prominent peaks and their

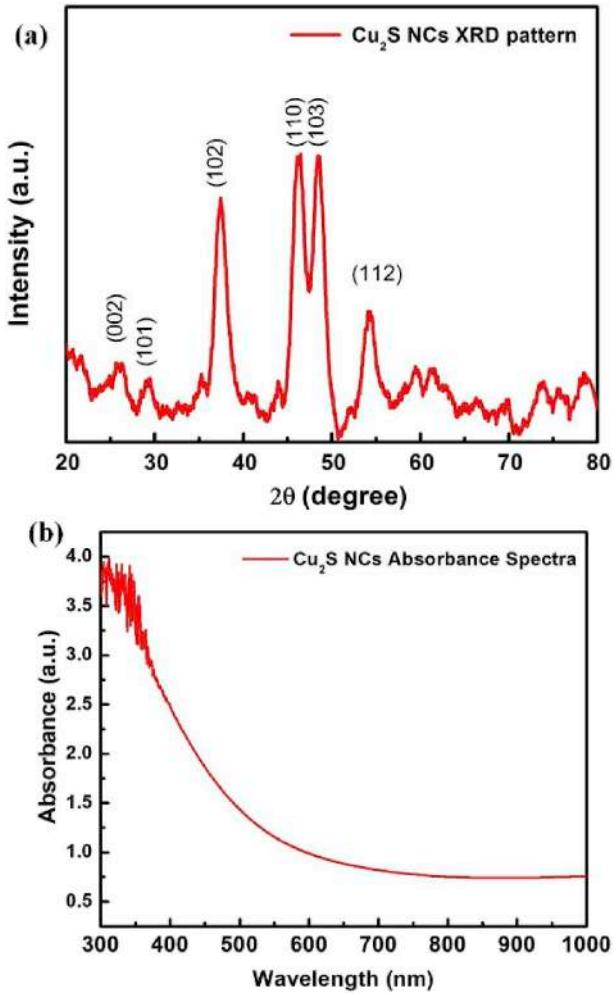

Fig. 1. (a) XRD pattern and (b) UV–Vis.–NIR absorption spectra of as synthesized Cu_2S NCs.

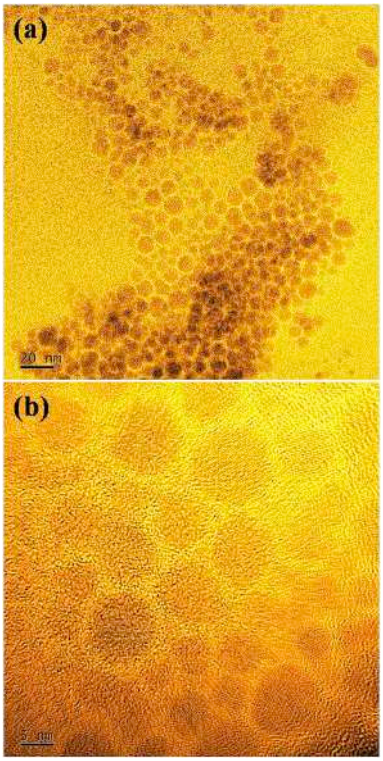

Fig. 2. (a–b) HRTEM images of as synthesized Cu_2S NCs.

corresponding 2θ value are in close agreement with the previous studies and conforms to the JCPDS file no.00-026-1116 [30,38]. This confirms the hexagonal crystal structure of the as-synthesized Cu_2S NCs. The absence of additional peaks besides the peaks of Cu_2S NCs confirms that the adopted protocol yields the pure phase of Cu_2S NCs which is essential for the device fabrication. Fig. 1(b) depicts the UV–Vis.–NIR absorbance spectra (Shimadzu 1800) of dispersion of the synthesized Cu_2S NCs in ethanol (1 mg/ml). It can be clearly seen that the as-synthesized Cu_2S NCs has wide absorption spectrum up to 1000 nm covering a wide spectrum in UV–Vis.–NIR region and therefore it is capable of harnessing the major part of the solar spectrum [30].

However, to confirm morphology, particle size and their distribution, HRTEM images (Jeol's JEM-2200FS) of as-synthesized Cu_2S NCs have been taken. From Fig. 2(a) and (b), it is clearly seen that the particles are slightly elongated and possess uniform size distribution whose length and diameter are around 10–20 nm and 6–10 nm respectively. The crystallinity of the as-synthesized Cu_2S NCs with an inter-layer spacing of 0.198 nm replicates quite well with d-spacing of the (110) plane of Cu_2S NCs [31].

After confirming the phase purity and crystal structure, morphology

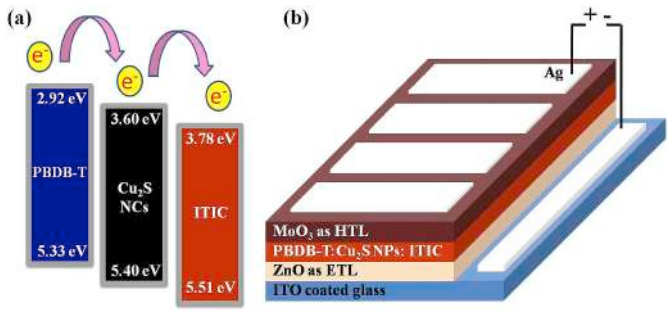

Fig. 3. (a) Energy levels of materials used in the solar cell device and (b) Schematic highlighting device architecture ITO/ZnO/PBDB-T: Cu_2S NCs: ITIC/MoO_3/Ag.

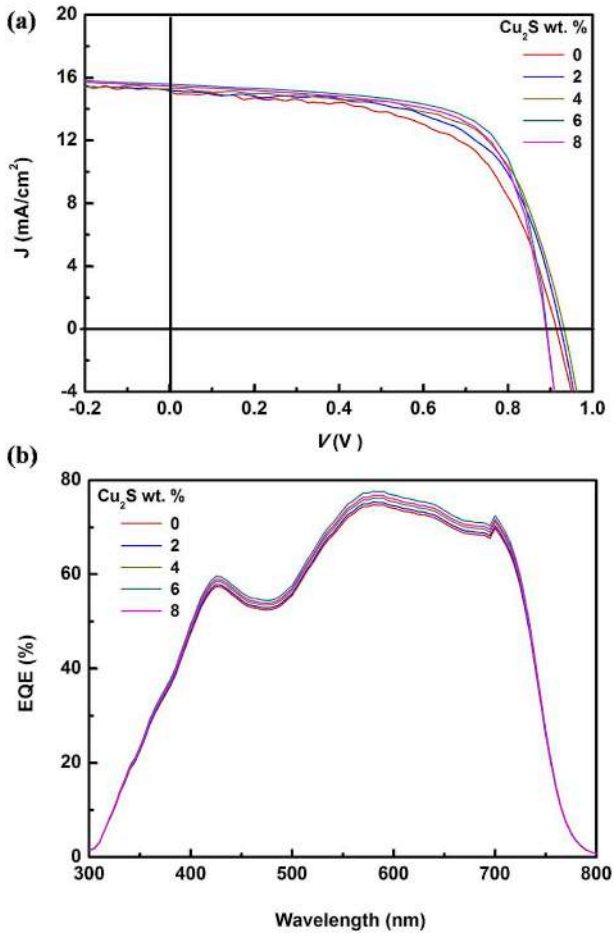

Fig. 4. (a) J – V characteristics under illumination (AM 1.5G, one sun) and (b) EQE spectra of PBDB-T: Cu_2S NCs: ITIC ternary OSCs with different wt % of Cu_2S NCs.

and optical properties of the synthesized Cu_2S NCs, nanocrystals based non-fullerene polymer solar cells were fabricated. As can be seen in Fig. 3(a), the conduction band of the Cu_2S lies between LUMO of donor polymer PBDB-T and non-fullerene ITIC, and therefore we hypothesize the enhancement in the device performance [39]. Devices were fabricated as shown in Fig. 3(b) whose procedure including the blend composition has been discussed in the experimental section.

Fig. 4(a) and (b) shows the J –V characteristics and EQE spectra of PBDB-T: Cu_2S NCs: ITIC ternary device as a function of wt % of Cu_2S NCs and corresponding performance parameters have been described in Table 1. As can be seen in Table 1, with the increase in the wt % of Cu_2S NCs, initially there is a slight increase in the V_{oc} till the concentration of Cu_2S NCs is 4 wt %. This is the expected outcome as it is well established that Voc depends on the energy difference between the HOMO of the donor polymer and the LUMO of the acceptor [40,41]. Addition of Cu_2S NCs generates the possibility of an energy level offset between the LUMO of the Cu_2S NCs and the HOMO of donor polymer which is better than the energy level offset between the LUMO of ITIC and the HOMO of the donor polymer [39]. However, with an increase in the concentration of Cu_2S NCs over 4 wt %, the surface defects of Cu_2S NCs dominates to create the shallow energy level trap in Cu_2S NCs leading to the disturbance of the energy level offset. Also, with the increase in wt % of Cu_2S NCs (till 6 wt %), there is a gradual increase in the current density (J_{sc}) and fill factor (FF). As a result, the PCE of the device increases from 8.24% to 9.53%. This is ~15% increase in the device PCE. This increase in the Jsc, FF and PCE can be understood by the observed decrease in the values of series resistance (R_s) and increase in the values of shunt resistance (R_{sh}) and can be attributed to PBDB-T, ITIC and Cu_2S

Table 1
Summary of J –V characteristics curves PBDB-T: Cu_2S NCs: ITIC devices with different wt % of Cu_2S NCs.

Cu_2S NCs wt %	V_{oc} (V)	Measured J_{sc} (mA/cm^2)	Calculated J_{sc}[a] (mA/cm^2)	FF (%)	PCE Best (%)[b]	R_s (Ωcm^2)	R_{sh} (Ωcm^2)
0%	0.91	15.11	15.07	59.45	8.24 (8.18)	9.36	234.07
2%	0.92	15.20	15.19	62.36	8.74 (8.69)	8.17	412.68
4%	0.93	15.31	15.36	64.38	9.18 (9.11)	8.09	465.78
6%	0.88	15.59	15.65	69.45	9.53 (9.45)	4.51	865.14
8%	0.88	15.48	15.48	68.11	9.27 (9.22)	4.90	728.73

[a] Calculated from EQE data.
[b] Average of the five devices in parentheses.

NCs charge transfer type interaction by considering that the added Cu_2S NCs may bind with PBDB-T: ITIC via dipole-dipole interaction and form a charge transfer complex (CTC) [30,35]. Upon further addition of Cu_2S NCs beyond 6 wt %, there is a decrease in the J_{sc} and FF. This leads to the decrease in PCE which might be due to the agglomeration of Cu_2S NCs in the matrix owing to less CTC formation. It can be said that the agglomeration of Cu_2S NCs increases R_s and decreases R_{sh}. EQE spectra also shows a similar trend and resemble with the trend observed in J-V curves. Calculated values of J_{sc} from EQE are shown in Table 1. However, to visualize complete picture, we have done intensity dependent photo-EIS measurements and discussed that in the subsequent section.

The incident light intensity dependent EIS spectra of both reference device (Cu_2S NCs, 0 wt %) as well as the best performing device (Cu_2S NCs, 6 wt %) are highlighted in Fig. 5 (a) and (b) respectively. It is apparently evident that in both the cases, photo-EIS spectra consist of only one semi-circle and can be fitted by a simple R_{rec}*C_μ equivalent circuit, where R_{rec} is a recombination resistance (R_{rec}) and C_μ is the chemical capacitance (C_μ). For attaining the proper fit, capacitor element has been replaced by commonly used constant phase elements (CPE) which gives a distribution of circuit element values in an equivalent circuit to account for any spatial inhomogeneity in the photoactive layer. For an ideal capacitor of capacitance C, the impedance is given by Eq (1) and in the case of a CPE, it is rather characterized by Eq (2) [42]. From the above equations, it is apparent that CPE is equivalent to capacitance. If P equals 1, then Eq (2) is identical to Eq (1). In the study, the CPE exponent (P) is varied from 0.85 to 1 and is well within the acceptable values.

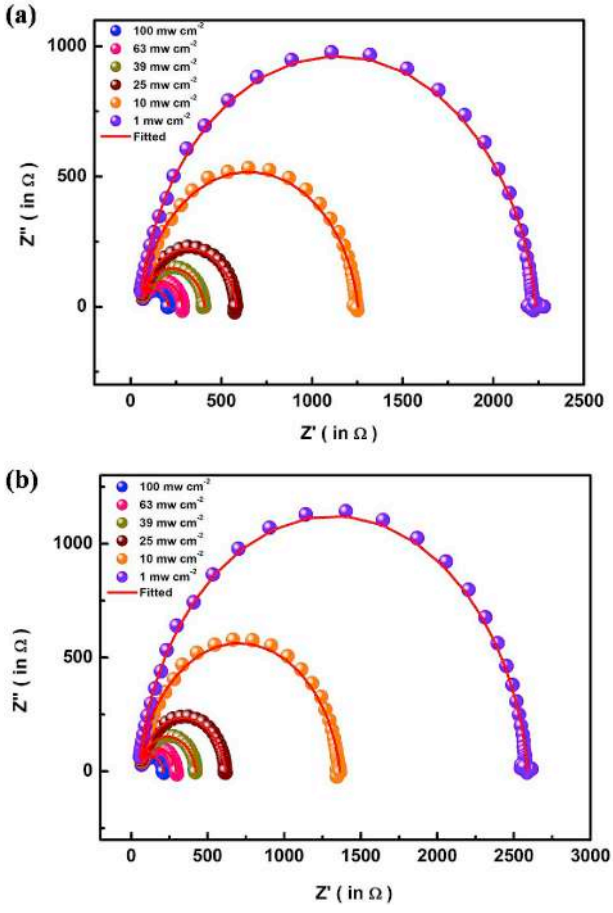

Fig. 5. Nyquist plots of PBDB-T: Cu_2S NCs: ITIC ternary OSCs under different white light illumination intensities with (a) 0 wt % of Cu_2S NCs and (b) 6 wt % of Cu_2S NCs.

$$Z_C = {}^{1}/_{i\omega c} \quad (1)$$

$$Z_{CPE} = {}^{1}/_{CPE\,(i\omega)^P} \quad (2)$$

Before analyzing the photo-EIS data, it is essential to mention here that there are basically three different ways of calculating the order of recombination using EIS data: 1) using exponent of the recombination resistance as function of V_{oc} 2) using exponent of the recombination resistance and chemical capacitance as function of V_{oc} 3) slope of $\tau \propto n^{-\delta}$ [42]. We will discuss all the above the cases in the context of the reference device (Cu_2S NCs, 0 wt %) and the best performing device (Cu_2S NCs, 6 wt %) [42].

From Fig. 6(a) and (b), it can be observed that with an increase in V_{oc}, the resistance and capacitance changes exponentially. Thus, recombination resistance and chemical capacitance can be fitted as a function of V_{oc} using the exponential laws mentioned in Eqs (3) and (4) [43]. This will give the insight about recombination processes within the devices. For the reference device (Cu_2S NCs, 0 wt %), obtained values of α and β are 0.30 and 0.83 respectively. However, for the best performing device (Cu_2S NCs, 6 wt %) α and β are 0.38 and 0.92 respectively. As discussed above, impedance measurements allow us to establish a direct relation between the order of recombination (λ) and exponents of resistance dependences on V_{oc} (β) and are given by Eq (5). Value of λ is 1 for trap-assisted recombination and is 2 for bimolecular recombination. In the present study, the order of recombination (λ) for reference device (Cu_2S NCs, 0 wt %) and for the best performing device (Cu_2S NCs, 6 wt %) are 1.66 and 1.84 respectively [43]. Thus, in both the cases, recombination losses are due to both trap-assisted recombination and bimolecular recombination [42]. However, it can be clearly observed that in the case of Cu_2S NCs 6 wt %, there are less trap-assisted recombination which could be due to the facilitation of charge transfer from PBDB-T to ITIC through Cu_2S NCs. Thus, the presence of Cu_2S NCs improves the device performance by minimizing the trap-assisted recombination.

$$R_{rec} \propto \exp(-\beta Voc/K_BT) \quad (3)$$

$$C\mu \propto \exp(\alpha Voc/K_BT) \quad (4)$$

$$\lambda = 2\beta \quad (5)$$

$$\lambda = \frac{\beta}{\alpha} \quad (6)$$

Order of recombination can also be calculated by using an exponent of the recombination resistance and chemical capacitance as a function

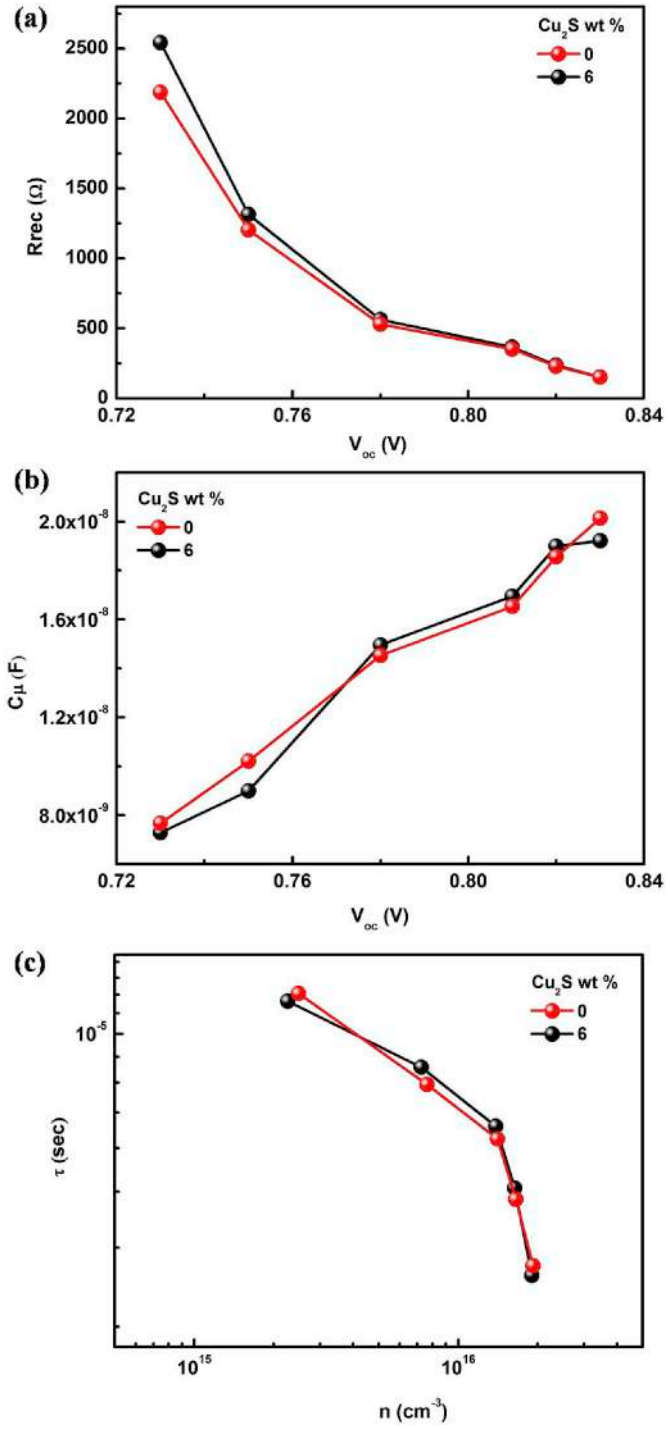

Fig. 6. (a) Recombination resistance (R_{rec}) as a function of V_{oc}, (b) Chemical capacitance (C_μ) as a function of V_{oc} and (c) Carrier life time as a function of the photo-generated carrier density of PBDB-T: Cu_2S NCs: ITIC ternary OSCs with 0 wt % and 6 wt % of Cu_2S NCs.

of V_{oc} using Eq (6). Recombination process can be thought of as a multiple trapping mechanisms. Here, trapped holes can either recombine with electrons at the acceptor levels or get retrapped at an exponential tail of donor states [43]. In the present study, the order of recombination (λ) using Eq (6) for reference device (Cu_2S NCs, 0 wt %) and for the best performing device (Cu_2S NCs, 6 wt %) are 2.76 and 2.44 respectively. This means that multiple trapping recombinations are less pronounced in the case of best performing device (Cu_2S NCs, 6 wt %).

To calculate the order of recombination using $\tau \propto n^{-\delta}$, we need to calculate recombination time and carrier density [44]. Response time representative of the recombination processes is calculated from the characteristic frequency (ω) at the top of the arc, where $2\pi\omega = 1/\tau$ [45,46]. For both the devices, effective recombination time (τ) range in the order of 10^{-5} to 10^{-6} s. Additionally, the charger carrie density (n) can be estimated from the chemical capacitance (C_μ) using Eq (7).

$$n = \frac{1}{e}\int_0^{Voc} C\mu\,(V)dv \tag{7}$$

$$\tau \propto n^{-\delta} \tag{8}$$

$$\lambda = (1 + \delta) \tag{9}$$

A graph between carrier lifetime versus photo-generated carrier density is represented by Fig. 6(c). All the curves in the graph show decay dynamics that follow a power law trend mentioned in Eq (8). The order of recombination (λ) can be obtained value from slope (δ) by using the relation given in Eq (9). In both the cases, it was observed that the order of recombination is ~2 suggesting that bimolecular recombination is the prominent loss mechanism [44].

In order to investigate the topology of the photoactive films, binary and ternary blends of PBDB-T:Cu_2S:ITIC is spin casted over the ITO substrate and AFM height images were captured and is represented in Fig. 7. Film in Fig. 7(a) represents the topology of binary photoactive blend which shows clusters with many aggregated domains and found to possess root mean square (RMS) surface roughness of 2.32 nm. This RMS surface roughness decreases with the increase of wt % of Cu_2S in the photoactive blend and further increases after some optimum concentration of Cu_2S in the blend. Similar trend has been observed in the previous studies related to incorporation of the NCs in OSCs [47]. The values of RMS surface roughness for different concentration of Cu_2S viz. 2 wt %, 4 wt %, 6 wt % and 8 wt % blends are found to be 2.18 nm, 2.09 nm, 1.83 nm and 1.99 nm respectively. Fig. 7(b) and (c) represents the 3D height images of the film made up of blend with 6 wt % and 8 wt % Cu_2S NCs while other images are attached in the supplementary information (S1). This change in the trend of surface roughness of the film with 8 wt % Cu_2S in the photoactive blend hampers the performance of the cell and supports the hypothesis of the agglomeration of Cu_2S in the blend.

4. Conclusion

We have successfully demonstrated Cu_2S NCs based non-fullerene ternary polymer solar cells. The devices were fabricated in an inverted geometry having a structure ITO/ZnO/PBDB-T: Cu_2S NCs: ITIC/MoO_3/Ag. It has been found that addition of Cu_2S NCs improves the performance parameters and PCE. PCE of ~9.6% has been achieved for the devices with 6 wt % of Cu_2S NCs. The improvement in the performance parameters has been explained on the basis of the light intensity dependent photo-EIS measurements which suggest that there are less trap-assisted recombination in the case of the best-performing device (Cu_2S NCs 6 wt %) due the facilitation of charge transfer from PBDB-T to ITIC through Cu_2S NCs.

Acknowledgments

GL thanks Dr. Bharat Kale, Director, Center for Materials for Electronics Technology (C-MET), Pune and Dr. Sudhir Arbuj, Scientist (C-MET, Pune) for their inputs in the synthesis of Cu_2S nanocrystals. GL also thanks management of Shiksha Mandal, Wardha and Principal, Jankidevi Bajaj College of Science (Autonomous), Wardha for providing central instrumentation facility to characterize the material. All the authors agreed on the results and given approval to the manuscript. The authors declare that there is no conflict of interest regarding the publication of this paper.

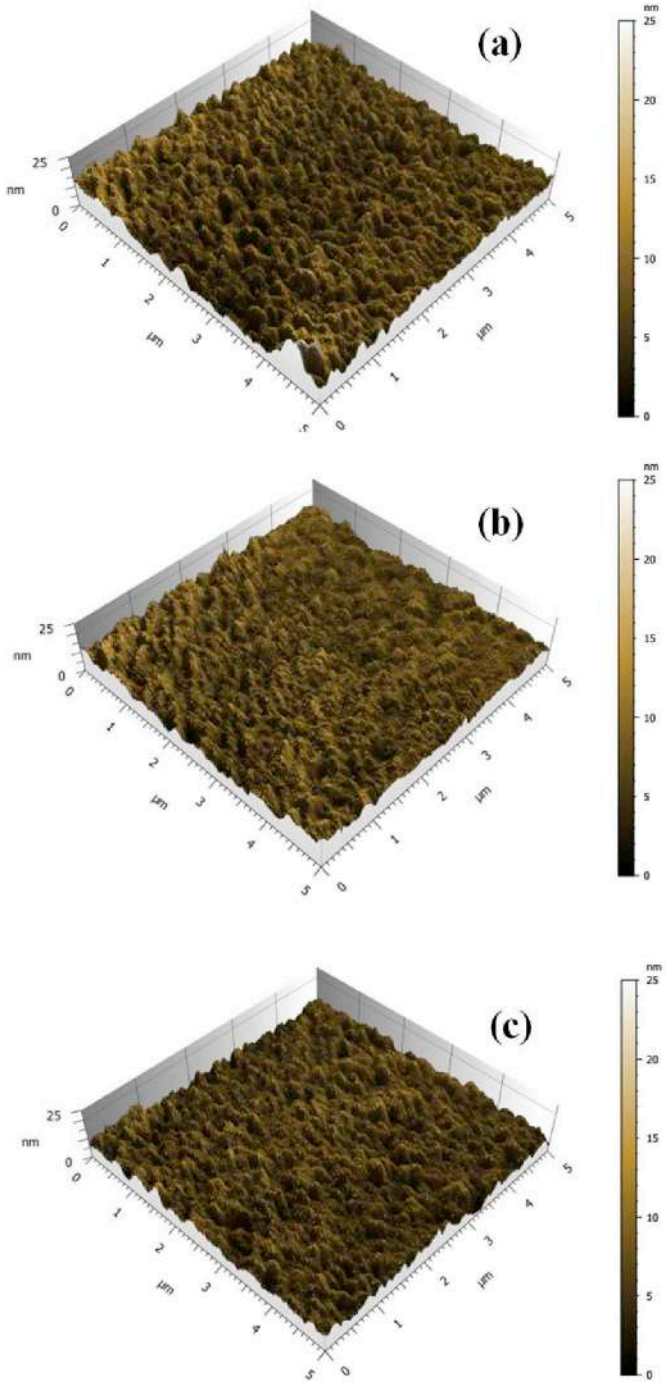

Fig. 7. AFM height images of the films made from the photoactive blend of PBDB-T:Cu_2S:ITIC with (a) 0 wt % Cu_2S NCs, (b) 6 wt % Cu_2S NCs and (c) 8 wt % Cu_2S NCs.

Appendix A. Supplementary data

Supplementary data to this article can be found online at https://doi.org/10.1016/j.cap.2019.01.006.

References

[1] B. Oregan, M. Gratzel, Nature 353 (1991) 737.
[2] G. Yu, J. Gao, J.C. Hummelen, F. Wudl, A.J. Heeger, Science 270 (1995) 1789.
[3] M.M. Lee, J. Teuscher, T. Miyasaka, T.N. Murakami, H.J. Snaith, Science 338 (2012) 643.
[4] J.H. Noh, S.H. Im, J.H. Heo, T.N. Mandal, S.I. Seok, Nano Lett. 13 (2013) 1764.
[5] N. Jain, N. Chandrasekaran, A. Sadhanala, R.H. Friend, C.R. McNeill, D. Kabra, J. Mater. Chem. A 5 (2017) 24749.
[6] A.K. Kyaw, D.H. Wang, V. Gupta, J. Zhang, S. Chand, G.C. Bazan, A.J. Heeger, Adv. Mater. 25 (2013) 2397.
[7] V. Gupta, A.K. Kyaw, D.H. Wang, S. Chand, G.C. Bazan, A.J. Heeger, Sci. Rep. Uk 3 (2013).
[8] J.F. Yan, B.R. Saunders, RSC Adv. 4 (2014) 43286.
[9] S. Gunes, H. Neugebauer, N.S. Sariciftci, Chem. Rev. 107 (2007) 1324.
[10] G. Dennler, R. Gaudiana, C.J. Brabec, Abstr. Pap. Am. Chem. Soc. 238 (2009).
[11] Y.H. Liu, J.B. Zhao, Z.K. Li, C. Mu, W. Ma, H.W. Hu, K. Jiang, H.R. Lin, H. Ade, H. Yan, Nat. Commun. 5 (2014).
[12] W.C. Zhao, D.P. Qian, S.Q. Zhang, S.S. Li, O. Inganas, F. Gao, J.H. Hou, Adv. Mater. 28 (2016) 4734.
[13] Y.Z. Lin, J.Y. Wang, Z.G. Zhang, H.T. Bai, Y.F. Li, D.B. Zhu, X.W. Zhan, Adv. Mater. 27 (2015) 1170.
[14] Z.C. He, B. Xiao, F. Liu, H.B. Wu, Y.L. Yang, S. Xiao, C. Wang, T.P. Russell, Y. Cao, Nat. Photon. 9 (2015) 174.
[15] Q.Q. Pan, S.B. Li, Y. Wu, Y. Geng, M. Zhang, Z.M. Su, Org. Electron. 53 (2018) 308.
[16] Y.K. Yang, Z.G. Zhang, H.J. Bin, S.S. Chen, L. Gao, L.W. Xue, C. Yang, Y.F. Li, J. Am. Chem. Soc. 138 (2016) 15011.
[17] W.C. Zhao, S.S. Li, H.F. Yao, S.Q. Zhang, Y. Zhang, B. Yang, J.H. Hou, J. Am. Chem. Soc. 139 (2017) 7148.
[18] F.W. Zhao, S.X. Dai, Y.Q. Wu, Q.Q. Zhang, J.Y. Wang, L. Jiang, Q.D. Ling, Z.X. Wei, W. Ma, W. You, C.R. Wang, X.W. Zhan, Adv. Mater. 29 (2017).
[19] X. Xu, T. Yu, Z. Bi, W. Ma, Y. Li, Q. Peng, Adv. Mater. 30 (2018) 1703973.
[20] L. Meng, Y. Zhang, X. Wan, C. Li, X. Zhang, Y. Wang, X. Ke, Z. Xiao, L. Ding, R. Xia, Science (2018) 2612.
[21] Y. Cui, H.F. Yao, B.W. Gao, Y.P. Qin, S.Q. Zhang, B. Yang, C. He, B.W. Xu, J.H. Hou, J. Am. Chem. Soc. 139 (2017) 7302.
[22] M.M. Li, K. Gao, X.J. Wan, Q. Zhang, B. Kan, R.X. Xia, F. Liu, X. Yang, H.R. Feng, W. Ni, Y.C. Wang, J.J. Peng, H.T. Zhang, Z.Q. Liang, H.L. Yip, X.B. Peng, Y. Cao, Y.S. Chen, Nat. Photon. 11 (2017) 85.
[23] J.Q. Zhang, Y.J. Zhang, J. Fang, K. Lu, Z.Y. Wang, W. Ma, Z.X. Wei, J. Am. Chem. Soc. 137 (2015) 8176.
[24] Y.J. Zhang, D. Deng, K. Lu, J.Q. Zhang, B.Z. Xia, Y.F. Zhao, J. Fang, Z.X. Wei, Adv. Mater. 27 (2015) 1071.
[25] Q.S. An, F.J. Zhang, J. Zhang, W.H. Tang, Z.B. Deng, B. Hu, Energy Environ. Sci. 9 (2016) 281.
[26] R. Sharma, H. Lee, V. Gupta, H. Kim, M. Kumar, C. Sharma, S. Chand, S. Yoo, D. Gupta, Org. Electron. 34 (2016) 111.
[27] L.Y. Lu, M.A. Kelly, W. You, L.P. Yu, Nat. Photon. 9 (2015) 491.
[28] R. Yu, H. Yao, J. Hou, Adv. Energy Mater. 8 (2018) 1702814.
[29] H.C. Liao, C.S. Tsao, T.H. Lin, M.H. Jao, C.M. Chuang, S.Y. Chang, Y.C. Huang, Y.T. Shao, C.Y. Chen, C.J. Su, U.S. Jeng, Y.F. Chen, W.F. Su, ACS Nano 6 (2012) 1657.
[30] S.R. Gollu, R. Sharma, G. Srinivas, S. Kundu, D. Gupta, Org. Electron. 15 (2014) 2518.
[31] R. Sharma, S. Bhalerao, D. Gupta, Org. Electron. 33 (2016) 274.
[32] B.J. Richardson, L.Z. Zhu, Q.M. Yu, Sol. Energy Mater. Sol. Cell. 116 (2013) 252.
[33] C.Y. Liu, Z.C. Holman, U.R. Kortshagen, Nano Lett. 9 (2009) 449.
[34] G. Itskos, A. Othonos, T. Rauch, S.F. Tedde, O. Hayden, M.V. Kovalenko, W. Heiss, S.A. Choulis, Adv. Energy Mater. 1 (2011) 802.
[35] M.T. Khan, A. Kaur, S.K. Dhawan, S. Chand, J. Appl. Phys. 110 (2011).
[36] Y. Wu, C. Wadia, W.L. Ma, B. Sadtler, A.P. Alivisatos, Nano Lett. 8 (2008) 2551.
[37] Y.M. Sun, J.H. Seo, C.J. Takacs, J. Seifter, A.J. Heeger, Adv. Mater. 23 (2011) 1679.
[38] S. Li, H.Z. Wang, W.W. Xu, H.L. Si, X.J. Tao, S.Y. Lou, Z.L. Du, L.S. Li, J. Colloid Interface Sci. 330 (2009) 483.
[39] M. Wright, A. Uddin, Sol. Energy Mater. Sol. Cell. 107 (2012) 87.
[40] H.X. Zhou, L.Q. Yang, S. Stoneking, W. You, Acs Appl. Mater. Interfaces 2 (2010) 1377.
[41] Z.T. Liu, M.F. Lo, H.B. Wang, T.W. Ng, V.A.L. Roy, C.S. Lee, S.T. Lee, Appl. Phys. Lett. 95 (2009) 227.
[42] W.L. Leong, S.R. Cowan, A.J. Heeger, Adv. Energy Mater. 1 (2011) 517.
[43] P.P. Boix, J. Ajuria, R. Pacios, G. Garcia-Belmonte, J. Appl. Phys. 109 (2011) 074514.
[44] A. Guerrero, N.F. Montcada, J. Ajuria, I. Etxebarria, R. Pacios, G. Garcia-Belmonte, E. Palomares, J. Mater. Chem. A 1 (2013) 12345.
[45] T.M. Clarke, C. Lungenschmied, J. Peet, N. Drolet, A.J. Mozer, Adv. Energy Mater. 5 (2015) 1401345.
[46] R. Sharma, V. Gupta, H. Lee, K. Borse, R. Datt, C. Sharma, M. Kumar, S. Yoo, D. Gupta, Org. Electron. 62 (2018) 441.
[47] B.J. Richardson, L. Zhu, Q. Yu, Sol. Energy Mater. Sol. Cell. 116 (2013) 252.